

Robustness of Topological Order in the Toric Code with Open Boundaries

Amit Jamadagni,^{1,*} Hendrik Weimer,¹ and Arpan Bhattacharyya^{2,3,†}

¹*Institut für Theoretische Physik, Leibniz Universität Hannover, Appelstraße 2, 30167 Hannover, Germany.*

²*Center for Gravitational Physics, Yukawa Institute for Theoretical Physics, Kyoto University, Kyoto 606-8502, Japan.*

³*Department of Physics and Center for Field Theory and Particle Physics, Fudan University, 220 Handan Road, 200433 Shanghai, P. R. China.*

We analyze the robustness of topological order in the toric code in an open boundary setting in the presence of perturbations. The boundary conditions are introduced on a cylinder, and are classified into condensing and non-condensing classes depending on the behavior of the excitations at the boundary under perturbation. For the non-condensing class, we see that the topological order is more robust when compared to the case of periodic boundary conditions while in the condensing case topological order is lost as soon as the perturbation is turned on. In most cases, the robustness can be understood by the quantum phase diagram of a equivalent Ising model.

I. INTRODUCTION

One of the main challenges in constructing a quantum computer has been to protect its qubits from decoherence. To overcome this challenge focus has shifted to topological quantum computation¹⁻³, where the information is naturally protected against local perturbation. In topological quantum computation, the information is encoded in the topological degrees of the freedom of the underlying system, the main ingredients of which are “anyons” which are certain type of topological excitations characterized by fractional or non-abelian statistics. These excitations can be found in certain topological phases of matter which are mainly characterized by long-range or short-range entanglement and have ground state degeneracy, gapless edge states as the signatures³⁻⁶.

In this article, we investigate the robustness of the toric code Hamiltonian in the presence of open boundaries. Our interest in open boundary conditions is twofold: On the one hand, possible experimental realizations of the toric code⁷⁻¹⁸ will be much easier to implement for open boundaries than on a torus. On the other hand, it has been known that boundaries play an important role in the context of classifying different phases of matter. E.g., various insulators with different symmetry breaking property separated by gapped domain wall exhibit rich physics in the low energy regime compared to a single insulating phase. With the introduction of domain walls in the context of topological order much has been studied on how two different topological phases can be connected with each other through a boundary^{19,20}, not only allowing the classification of phases via anyon condensation²¹ but also realizing the domain wall as a means for quantum computation²²⁻²⁴. More importantly, from a practical point of view, these open boundary topologies play an important role in realizing ideas experimentally, as we have to deal with a finite system and also more trivial topologies. A systematic classification of boundaries in the context of Quantum Double models, including the domain wall classification has been discussed in Ref. 19.

The notion of boundaries have also been discussed in the context of Levin-Wen string net models²⁵ in Ref. 20 using the language of category theory.

Therefore, from a practical point of view it is important to understand the robustness of topological order in an open boundary setting under external perturbation. The robustness of toric code, in a periodic boundary setting, has been extensively studied under various perturbations²⁶⁻²⁹. In this paper we address the robustness in the context of open boundaries given its importance as discussed above. We begin with a brief introduction of the toric code in a periodic boundary setting in Sec. II, we review the open boundary conditions in Sec. III and consider them in the presence of perturbation. We also review the map between the toric code under perturbation in an open boundary setting to an equivalent Ising model. In Sec. IV, using the above equivalence we gain an insight into the robustness of topological order. In Sec. V, we extend the discussion of Sec. IV, by numerically studying various signatures of topological order in the exact model. We observe that Topological Entanglement Entropy acts as a good signature in detecting the phase transition, while a method based on Minimally Entangled States fails to capture the transition.

II. TOPOLOGICAL ORDER IN THE TORIC CODE

We briefly review the physics behind the toric code model³⁰, the simplest case of more general class of models known as quantum double models¹⁹. Consider a square lattice with vertices denoted by v , the faces denoted by p and with spins on edges of the lattice on a torus, as in Fig. 1. The Hamiltonian of the toric code is given by,

$$H_{toric} = - \sum_v A_v - \sum_p B_p \quad (1)$$

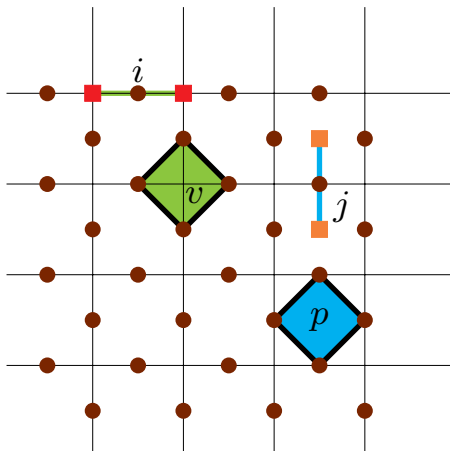


Figure 1. Toric code model. The A_v operator, denoted by the green diamond, acts on the spins attached to the vertex v . The B_p operator, denoted by the blue diamond, acts on the spins which form the face p . The red squares denote A_v violations which appear in pairs at the end of the ribbon operator generated by σ_z^i . Similarly, the orange squares denote B_p violations, which also appear in pairs at the end of the ribbon operator generated by σ_x^j .

where $A_v = \prod_i \sigma_x^i$ and $B_p = \prod_j \sigma_z^j$.

The ground state, $|\psi_{gs}\rangle$, of the toric code Hamiltonian is a simultaneous ground state of all the A_v and B_p operators, implying the relations

$$\begin{aligned} A_v |\psi_{gs}\rangle &= |\psi_{gs}\rangle, \forall v, \\ B_p |\psi_{gs}\rangle &= |\psi_{gs}\rangle, \forall p. \end{aligned} \quad (2)$$

The excitations in the model are given by A_v violations and B_p violations, which are generated by σ_z and σ_x operators respectively, as shown in Fig. 1. We note that the ground state manifold is four-fold degenerate as fusing the excitations along non-trivial topological loops of the torus projects us back into an orthogonal state that satisfies Eq. 2 as well. The properties of the excitations and the ground state degeneracy are both signatures of topological order in the system. One other key signature of topological order is the so called non-vanishing regularization independent constant term in the entanglement entropy for the ground state known as Topological Entanglement Entropy (TEE). For toric code it is given by $\log 2$. It has been shown that TEE is related to the quantum dimensions of quasi-particle excitations^{31,32}, and hence capture the essence of the topological order. In this paper, we will extensively use TEE as a signature to quantify the robustness of topological order and thereby use it to predict the topological phase transitions under perturbations of the toric code in an open boundary setting.

III. GAPPED BOUNDARIES OF THE TORIC CODE

In the above section, we have reviewed the well-known idea of topological order in case of toric code on a torus. In this section we present a brief review of various open boundary scenarios in the case of toric code, which have been extensively discussed in Refs. 19, 20, and 33. We specifically review the interfaces with the toric code on one side and the vacuum on the other.

A. Boundary classification and the system Hamiltonian

We begin by reviewing the classification of the boundaries which has been presented in Ref. 19 for general quantum double models. Given a quantum double $D(G)$, characterized by a finite group G (abelian or non abelian) the possible boundaries are classified by the subgroups K of G . In the case of toric code, which is equivalent to $D(Z_2)$ we look at the subgroups of Z_2 which are given by $\{e\}, Z_2$ where e is the identity of the group Z_2 . We will refer to the case where the boundary is decorated with $\{e\}$ ($K=\{e\}$), as identity as boundary and the case where the boundary is decorated with Z_2 ($K=Z_2$), as group as boundary.

To be explicit, we consider the toric code on a cylinder. We define the Hamiltonian of the system by adding additional boundary terms to the bulk Hamiltonian, the latter being the familiar toric code model. Thus, the Hamiltonian has the form

$$H_{boundary} = H_{toric}^{bulk} - \sum_{i \in boundary} O_i. \quad (3)$$

For the case of identity as boundary, $K = \{e\}$, we have $O_i = B'_p$, where $B'_p = \prod_{i=1}^3 \sigma_z^i$, with i representing the spins on the boundary faces, as shown in Fig. 2(a). In the case of group as boundary, $K = Z_2$, we have $O_i = A'_v$ where $A'_v = \prod_{i=1}^3 \sigma_x^i$, with i now running over the spins at the boundary vertices, see Fig. 2(b).

Alternatively, boundaries can also be classified by the behavior of the excitations at the boundary. For a given quantum double model $D(G)$, the excitations are given by the irreducible representations of the centralizers of the conjugacy class of G . Given a choice of boundary, every excitation either vanishes and is called a condensing excitation, or it is retained at the boundary, which is known as the non-condensing excitation. Ref. 19 provides a mechanism to identify whether an excitation condenses at a particular choice of boundary. This condensing/non-condensing behavior of the excitation can be used to classify different boundary conditions. For instance, in the toric code with open boundaries, identity as boundary corresponds to A_v excitation condensing on the boundary, while group as boundary corresponds to B_p excitation condensing on the boundary, and vice-versa.

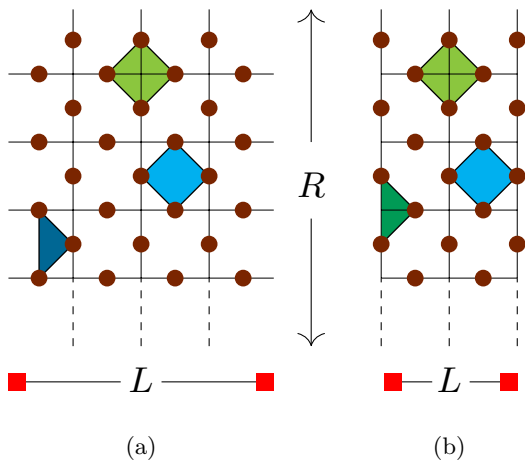


Figure 2. Toric code with open boundaries on a cylinder with length L and radius R . (a) Toric code with identity as boundary. (b) Toric code with group as boundary. The brown dots represent the physical spins, the light green diamond represents the A_v operator, the light blue diamond represents the B_p operator, and the dark blue half diamond represents the modified B'_p operator for identity as boundary in (a), and the dark green half diamond represents modified A'_v operator for group as boundary in (b).

For both the boundary cases, one of the ground states is given by

$$|\psi_{gs}\rangle_{boundary} = \mathcal{N} \prod_v (1 + A_v) |\mathbf{0}\rangle, \quad (4)$$

where $|\mathbf{0}\rangle = |00\dots 0\rangle$, $|0\rangle = \begin{pmatrix} 1 \\ 0 \end{pmatrix}$, \mathcal{N} is a normalization constant, and the product over v is modified to include the vertices depending on the boundary.

Our main goal is to study the robustness of topological order in an open boundary setting with respect to perturbations generated by magnetic fields applied in different directions. We lay a particular emphasis on identifying phase transitions between a topologically ordered phase (for weak perturbations) and a topologically trivial phase (for strong perturbations). We use different methods to identify various signatures of topological order to get a consistent picture. This way, our results also serve as a benchmark for the different methods to classify the topological properties of a system.

In our analysis, we are interested in the topological properties of an infinitely large system. While there are different ways how to approach the thermodynamic limit in the cylindrical geometry introduced in the previous section, we are interested in the case where the boundary contribution is extensive. Hence, we will focus on a quasi-1D geometry where the length L of the cylinder is finite, while the radius R diverges.

B. Perturbation in the presence of boundaries

We begin by studying the effect of perturbations of the form $\sum_i \sigma_z^i$, $\sum_i \sigma_x^i$ on the Hamiltonians generated by Eq. 3. In particular, we will investigate cases where one of two perturbations is present at a given time. We could have simultaneously turned both of them at the same time to get the full phase diagram, as in toric code on a torus^{34,35}, but we leave this investigation to the future.

1. Exact Hamiltonians

Given that we have two different boundary conditions and we consider two different types of perturbation, $\sum_i \sigma_x^i$ and $\sum_j \sigma_z^j$, we have the following cases:

1. In the first case, the perturbed Hamiltonian has the form

$$H_{idpx(grpz)} = H_{id(gr)} - h_{x(z)} \sum_i \sigma_{x(z)}^i. \quad (5)$$

Here, the perturbation commutes with the A_v (B_p) operator, and anti-commutes with the B_p (A_v) operator leading only to the B_p (A_v) violations. As we have seen in Sec. III A, we know that B_p (A_v) violations are contained in the identity (group) as boundary case. As the above violations are both non-condensing, they will give rise to the same effective non-condensing Ising Hamiltonian, which we shall discuss later in detail.

2. In the second case, the perturbed Hamiltonian is given by

$$H_{idpz(grpx)} = H_{id(gr)} - h_{z(x)} \sum_i \sigma_{z(x)}^i. \quad (6)$$

In this scenario, the perturbation commutes with the B_p (A_v) operator, and anti-commutes with the A_v (B_p) operator leading only to A_v (B_p) violations. Again, from the arguments laid out in Sec. III A, we know that A_v (B_p) violations condense in identity (group) as boundary case. As these violations are both condensing, they will both lead us to the same effective condensing Ising Hamiltonian.

2. Ising Hamiltonians

In the following, we map the above exact Hamiltonians to associated Ising Hamiltonians. We briefly motivate the map and leave the detailed explanation to Appendix A. We consider a situation where the energy cost of one type of excitation (i.e., either A_v or B_p) is set to infinity and hence, only the other type of excitation can be observed in the system³⁶. As in Ref. 36, we construct an equivalent

model, where the degrees of freedom are the excitations of the system and not the individual spins. As any vertex or plaquette can contain only one or zero excitations, it is natural to use Ising spin 1/2 variables to describe the effective model. In the bulk, each term of the perturbation creates two excitations on adjacent vertices (plaquettes), see Fig. 1, corresponding to an effective Ising interaction.

However, at the boundary the interaction is captured by the way the excitation behaves at the particular choice of boundary. For the case where excitations condense at the boundary, we can always create single excitations in the bulk, implying the spins in the excitation picture near the boundary can be flipped independently, resulting in the Hamiltonian

$$H_{ci} = -h \left(\sum_{i,j} \mu_i^x \mu_j^x + \sum_{k \in \text{boundary}} \mu_k^x \right) - \sum_i \mu_i^z \quad (7)$$

where H_{ci} refers to the Condensing Ising (CI) Hamiltonian with perturbation strength h . For the case where excitations do not condense on the boundary, the nearest neighbor Ising interaction between the excitations at the boundary is still intact, resulting in the Hamiltonian

$$H_{nci} = -h \sum_{i,j} \mu_i^x \mu_j^x - \sum_i \mu_i^z, \quad (8)$$

where H_{nci} refers to the Non Condensing Ising (NCI) Hamiltonian with the perturbation strength, h on the Ising interaction.

We verify the above intuitive picture by using the Controlled-NOT (CNOT) mechanism as in Ref. 36, which is presented in Appendix B. By performing the CNOT mechanism in the open boundary context, we observe that in addition to the Ising like interactions we have a vacancy and topological spin (non-local spin- $\frac{1}{2}$ associated to the non-trivial [non-local] loops which project into different ground states) as observed in the periodic boundary case^{36,37}. Let us summarize the main results from Appendix B, focusing on the periodic boundary of the cylinder in the context of group as boundary under $\sum_i \sigma_x^i$ perturbation (6). Using the CNOT map, we see that the interaction at the periodic boundary is captured by $-h \sum_{p',q'} \mu_{p'}^x \otimes L_x \otimes \mu_{q'}^x$, where p', q' are Ising spins on either side of the boundary with L_x given by

$$L_{x(z)} = \prod_{j \in L} \sigma_{x(z)}^j, \quad (9)$$

L being the shorter width of the cylinder. Similarly, we can extend the result to other Hamiltonians 5, 6 where the boundary is coupled by the non-trivial loop operator $L_{x(z)}$ as above. While the effect of these additional terms is irrelevant for the thermodynamic properties of the system, they are essential to capture the relation between a thermodynamic phase transition in the effective model and the associated breakdown of topological order.

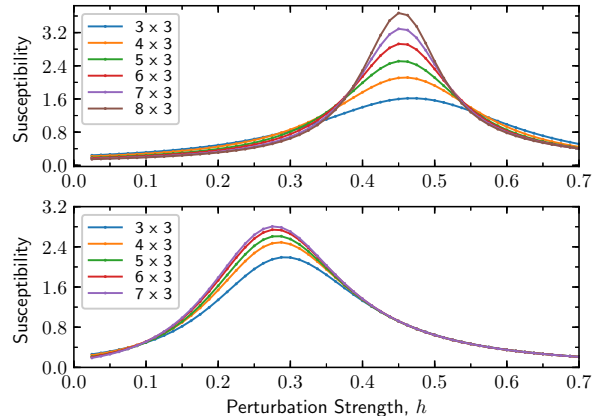


Figure 3. Susceptibility of the Ising model equivalent to the non-condensing case (Top) condensing case (Bottom)

IV. CHARACTERIZING THE PHASE TRANSITION: ISING MAP AND MAGNETIZATION

In this section we analyze the two Hamiltonians, (7) and (8), to gain an understanding of the phase transition in detail. We observe the behavior of magnetization, which acts as the order parameter, with respect to the strength parameter h .

A. Non Condensing case

We begin by studying the NCI Hamiltonian at different perturbation strengths. We note that as perturbation strength is increased, long ribbon operators (long strings with excitations at their ends) are penalized and shorter loops gain prominence which are captured by Ising interaction. Therefore we expect to capture a paramagnetic to a ferromagnetic transition and to gain an insight into the phase transition, we calculate the absolute of magnetization m , which is given by

$$m = \frac{1}{N} \sum_{i=1}^N \mu_i^x, \quad (10)$$

where N is the total number of spins. We denote the susceptibility by χ , which is given by

$$\chi = \frac{\partial m}{\partial h} \quad (11)$$

From Fig. 3, we infer that there is a phase transition occurring at some point between 0.4 and 0.5 as the susceptibility diverges with R . To precisely capture the transition we perform a finite size scaling analysis³⁸.

Finite Size scaling

The expression used for finite size scaling is given by

$$m = N^{-\beta/\nu} \tilde{f} \left([h - h_c] N^{1/\nu} \right), \quad (12)$$

where h_c is the critical strength, m is the magnetization, N is the system size, ν, β are the critical exponents, \tilde{f} is a scaling function chosen as a degree 6 polynomial. Here we know m, g, N and fit the data to determine the coefficients of the polynomial, \tilde{m} and g_c . From the fit, We infer that the critical strength is given by $h_c = 0.453 \pm 0.001$ and the critical exponents are given by, $\beta = 0.1 \pm 0.007$, $\nu = 1.131 \pm 0.013$ which are in good agreement with the critical exponents of the 2D Ising universality class ($\beta = 0.125$, $\nu = 1$).

We note that topological order under perturbation is more robust in the non-condensing scenario in comparison to the periodic boundary case, where the critical strength occurs at $h_c^{periodic} = 0.328^{35}$. This surprising result can be attributed to the role of quantum fluctuations in both cases. Crucially, the topologically ordered phase corresponds to the disordered phase of the Ising model (i.e., the paramagnet), and vice versa. In our cylindrical setup representing a quasi-1D system, the role of quantum fluctuations is stronger than on 2D setup on a torus. Hence, in the context of constructing a robust memory, it appears that is more beneficial to store a single qubit in a quasi-1D setup rather than two qubits on a torus.

B. Condensing case

We analyze the condensing case analogously to the non-condensing case. Observing the CI Hamiltonian (7), in the thermodynamic limit, we see that Z_2 symmetry of the Ising model is broken as soon as the perturbation is turned on. This is because of the localized excitations which appear at vertices/faces in bulk which share an edge with the boundary, Also, the topological coupling terms provide further insight into the breaking of ground state degeneracy, which is a signature of topological order.

In the presence of the perturbation, the effective Ising Hamiltonian including the topological coupling term is given by (cf. App. B)

$$H_{ci}^{eff} = - \sum_i \mu_i^z - h \left(\sum_{i,j} \mu_i^x \mu_j^x + \sum_{k \in boundary} \mu_k^x + \sum_{(p,q)} \mu_p^x \otimes L_x \otimes \mu_q^x \right). \quad (13)$$

We now perform a mean-field decoupling for the Ising model and look into the resulting coupling to the topological sector. Then, we obtain an effective topological

coupling of the form $h_{eff}^{MF} = h \langle \mu_p^x \rangle \langle \mu_q^x \rangle L_x$. In the condensing case, the presence of the Z_2 breaking terms lead to $\langle \mu_p^x \rangle \langle \mu_q^x \rangle \neq 0$ for any finite h . Hence, the topological degeneracy is lifted once the perturbation is turned on and topological order is destroyed. On the other hand, in the non-condensing case, we have $\langle \mu_p^x \rangle \langle \mu_q^x \rangle = 0$ for $h < h_c$. Consequently, the topological sector is decoupled from the Ising model and topological order remains intact. Strikingly, in the ferromagnetic phase, $h > h_c$, the expectation values become finite since they represent the order parameter of the ferromagnet. Again, this leads to a lifting of the topological degeneracy and a breakdown of topological order. Including the topological terms in the CNOT map therefore provides a deep insight into the connection between the thermodynamic transition in the effective Ising model and the associated breakdown of topological order.

As in the non-condensing case, we compute the magnetization to numerically verify the above claim. From Fig. 3, we observe that there is no divergence in the susceptibility with increase in the perturbation strength. Therefore, to further strengthen and numerically verify the above claim we revert back to the original model and study various signatures of topological order. As we have already established the non-condensing scenario, we use the topological signatures in the non-condensing case to benchmark our analysis of the condensing case.

V. CLOSER LOOK AT THE CONDENSING CASE

We analyze the following signatures to gain an insight into the robustness of topological order:

1. Breaking of the ground state degeneracy
2. Topological Entanglement Entropy
3. Minimally Entangled States (Two minima in topologically ordered phase to one in trivial phase)

A. Energy scaling

1. Identity as boundary

We begin by analyzing the ground state degeneracy of the Hamiltonian H_{idpz} , which we know has two degenerate ground states³⁹ at $h_x = 0$. In the thermodynamic limit, we expect the ground state degeneracy to break as soon as we turn on the perturbation, which we aim to observe in terms of the energy difference (ΔE). Using the fact that there is a phase transition in the non-condensing case, we compare Fig. 4 and Fig. 5, which depict the behavior of ΔE to gain an insight into the understanding of the condensing case. We see that in the non-condensing case as we approach the thermodynamic limit, there is a suppression in ΔE for $h < h_c$, which is as expected²⁶,

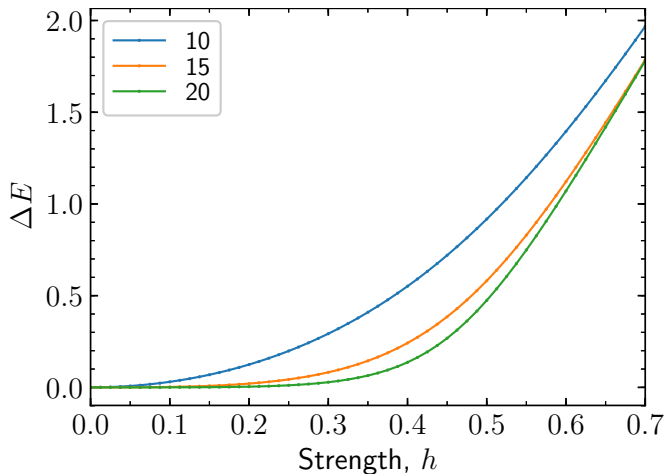


Figure 4. Energy Difference, ΔE , in the presence of perturbation for the non-condensing case (identity as boundary).

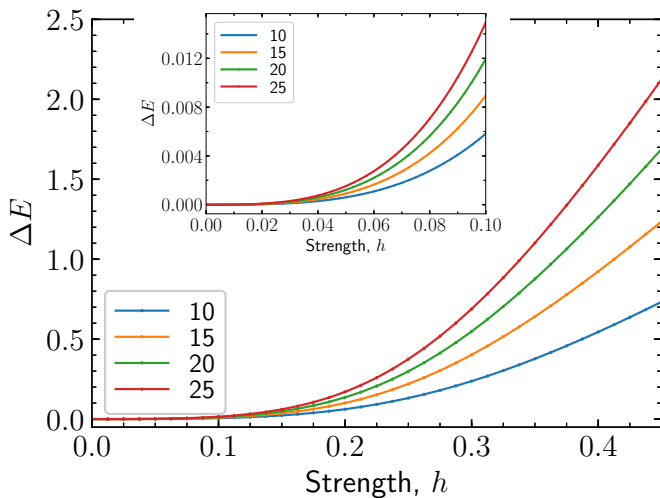


Figure 5. Energy Difference, ΔE , in the presence of perturbation for the condensing case with identity as boundary. (Inset) ΔE for strength range much closer to zero.

but in the condensing case, ΔE increases with perturbation strength as well with an increase in system size, with no suppression. Extrapolating the results to the thermodynamic limit, we can conclude that energy gap opens as soon as the perturbation is turned on.

2. Group as boundary

As a consistency check, we consider the Hamiltonian H_{grp} and compute ΔE , as expected the degeneracy is lifted as soon as the perturbation is turned on as in Fig. 6. Therefore, for the condensing class we conclude that $\Delta E > 0$ as soon as the perturbation is turned on, which strengthens the claim that for $h_x > 0$ the phase is broken, making it topologically trivial.

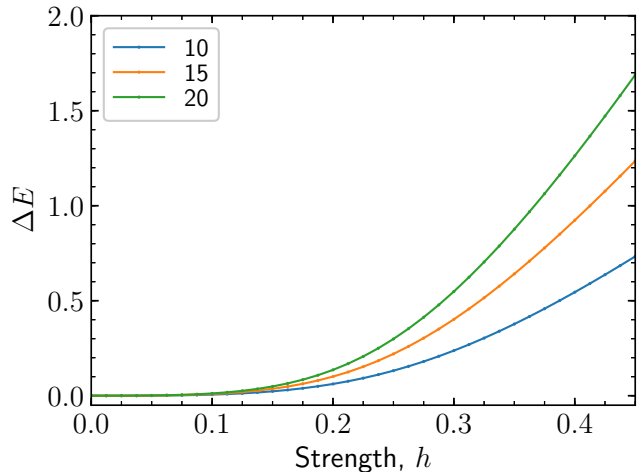


Figure 6. Energy Difference, ΔE , in the presence of perturbation for the condensing case with group as boundary, we observe that the nature of the graph is similar to the case of identity as boundary as in Fig. 5.

B. Topological Entanglement Entropy

One other key signature of topological order is the topological term in the entanglement entropy^{31,32}. Consider a region, say A , on the lattice, and denote the reduced density matrix by ρ_A . The von-Neumann entropy S_A given by $S_A = -\text{tr}(\rho_A \ln \rho_A)$ scales as following

$$S_A = a L_{cut} - \gamma \quad (14)$$

where L_{cut} is the length of the cut and γ is identified as the topological term and is called Topological Entanglement Entropy (TEE) which is a signature of topological order.

To compute γ , we consider a topologically non-trivial cut which winds around the surface of the cylinder as in the Fig. 7 and replicate the method used in Ref. 40. Note that the cut that we are employing is different than the ones used in Refs. 41 and 42, as our choice contains only a single boundary. The length of the region A , from which we extract the TEE, scales with R and the width of the region A is fixed. Therefore, in our case the above equation (14) changes to

$$S_A = a R - \gamma \quad (15)$$

consequently computing the entropy for different R and fitting S_A versus R gives us γ , which is the y-intercept of the fit.

1. Non-Condensing case

We first verify the already established fact of phase transition for the non-condensing class using TEE. Consider the non trivial cut as in the Fig. 7, either of the

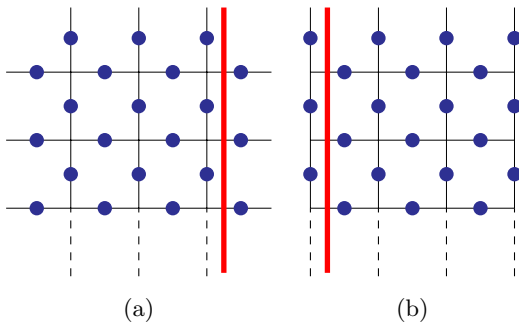


Figure 7. Different cuts used for the computation of entropy. (a) Cut for identity as boundary (b) Cut for group as boundary. The region used for the computation of entropy always includes the boundary and it can be either the region to the left or right of the cut. For computational purposes, we choose the region to the right of cut in (a) and left of the cut in (b) for computing the entropy.

boundary conditions can be considered with a suitable perturbation that results in a non-condensing scenario. Here we consider the Hamiltonian H_{idpx} and extract the TEE using Fig. 8(a), which is the y-intercept of the plot between S_A and R . We plot the TEE against the strength to identify the transition point as in the Fig. 8(b). From Fig. 8(b), we re-establish the fact that in the non-condensing case there is a phase transition from a ordered phase to a trivial phase as TEE scales from $\log 2$ to 0 with an increase in the perturbation strength. We also note that, numerically the critical strength from the TEE calculation is comparable to the exact results from the magnetization results. While we observe a dip in the TEE below $-\log(2)$, we attribute this to a finite size effect since it occurs close to the transition point, where finite size effects are particularly strong.

2. Condensing case

a. Identity as boundary

From the above case, it is clear that we can predict the presence of a transition point by observing the behavior of TEE. For the condensing case, in the earlier sections we argued that the phase is trivial as soon as the perturbation is turned on. To further consolidate the claim, we study the TEE behavior in the presence of perturbation for the condensing class. First we consider the Hamiltonian H_{idpz} and verify the results for the Hamiltonian H_{grpz} . As in the non condensing case, we consider a non-trivial cut along the surface of the cylinder, compute the entropy and extract the TEE for different perturbation strength. From Fig. 9, we observe that as soon as perturbation strength is turned on, TEE drops to zero thereby confirming the above mentioned picture.

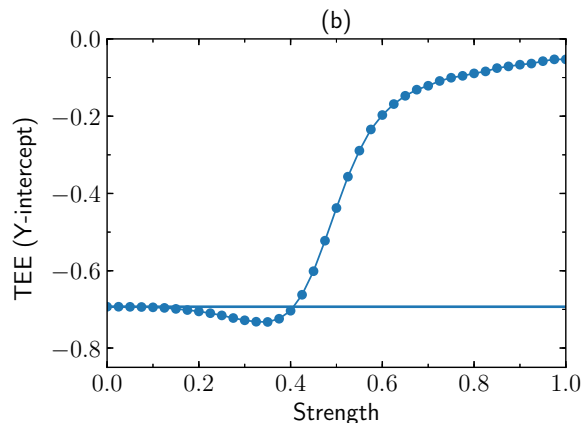
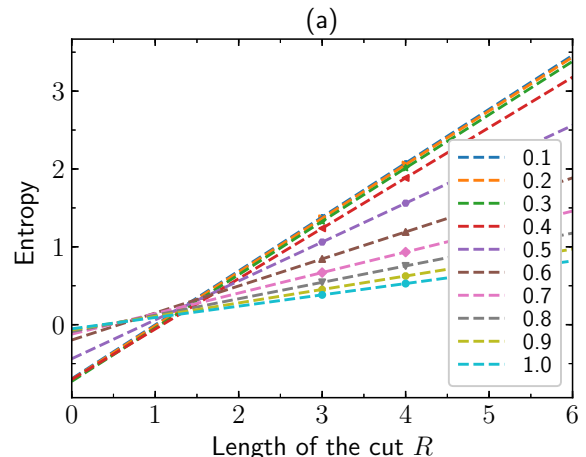


Figure 8. Extracting TEE in the non-condensing case. (a) For a given strength, we consider cuts of $R = 3, 4$ for computing the entropy, S_A , where region A is as in Fig. 7 and then fit S_A versus R to extract the TEE, which is the y-intercept of the fit. (b) TEE at different perturbation strengths. As the perturbation strength is increased, TEE scales from $\gamma = \log 2$ to $\gamma=0$, signaling a phase transition.

b. Group as boundary

We verify the conclusion from the above section by repeating the process of computing TEE for the condensing case with group as boundary. From Fig. 10, we observe that the behavior of TEE is same as above, which supports that for the condensing class, the system is topologically ordered at $h = 0$ and is trivial for $h > 0$.

C. Minimally Entangled States

In this section, we analyze the condensing case using Minimally Entangled States (MES). MES are very useful in the construction of the modular S -matrix, which is a key signature for topological order. The general outline of constructing the modular S matrix from MES has been

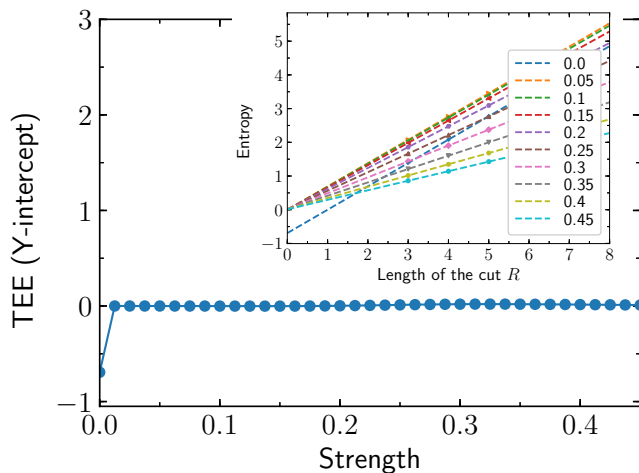


Figure 9. Extracting TEE in the condensing case, with identity as boundary. TEE remains zero as the strength is varied, only for $h = 0$ it is $\gamma = \log 2$. (Inset) Entropy versus the length of the cut (a non trivial cut equal to the radius of the cylinder), to extract the TEE (y-intercept) at each strength.

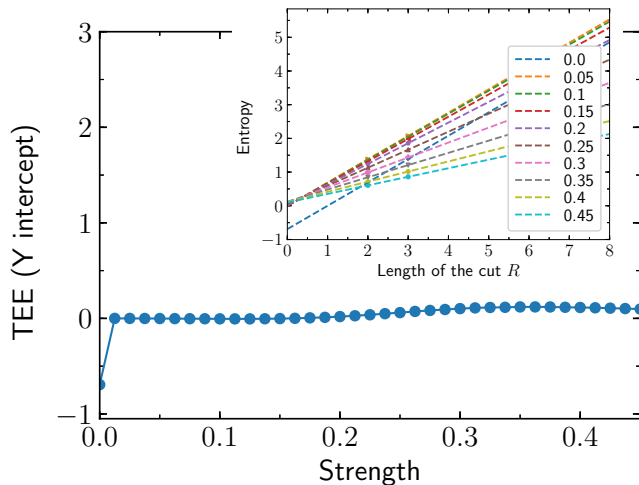


Figure 10. Extracting TEE in the condensing case, with group as boundary. The nature of TEE remains same as in the identity as boundary case.

discussed in Refs. 43–45. The idea of the MES is to compute states which are minimally entangled by observing the Renyi-2 entropy of the region which is trapped inside a non-trivial cut. In the case of cylinder, we have a single non-trivial cut which encircles the circumference of the cylinder (refer Fig. 7) and we use this to detect the MES, which are two in number for $h = 0$ ⁴³. As the number of Minimally Entangled States in trivial phase is one, we can use the change in MES, from two in topologically ordered state to one in the trivial phase, as a signature of phase transition. For completeness, we sketch the procedure below:

1. We start with the linear superposition of ground

states, say $|\psi_1\rangle, |\psi_2\rangle$ (starting at $h = 0$), $c_1 |\psi_1\rangle + c_2 e^{i\phi} |\psi_2\rangle$, where $c_2 = \sqrt{1 - c_1^2}$ and $0 \leq c_1 \leq 1$, $0 \leq \phi < 2\pi$.

2. We then find c_1, ϕ such that the renyi 2-entropy given by $S_2 = -\log(\text{Tr}(\rho_A^2))$ is minimized.
3. We plot the entropy parameterized by c_1, ϕ and estimate the nature of the entropy.
4. We observe that the minima occur at $\phi = 0, \pi$, so effectively we can minimize the entropy w.r.t c_1 either for $\phi = 0$ or $\phi = \pi$.
5. We repeat the above step for different system sizes and compute the critical strength in the thermodynamic limit by extrapolating $\frac{1}{R}$ versus h in the limit of $R \rightarrow \infty$.

We perform the above procedure for the condensing Hamiltonian H_{idpz} . As discussed above, we then compute the renyi-2 entropy of the wavefunction, $c_1 |\psi_1\rangle + c_2 e^{i\phi} |\psi_2\rangle$, either for $\phi = 0$ or $\phi = \pi$ and minimize w.r.t c_1 . Clearly, we can see the minimum shifting to $c_1 = 1$, as in Fig. 11, which implies that eventually we end up with just one state which further implies that the topological order is broken. By observing Fig. 12, we arrive at a critical strength h , for the corresponding system size which scales with R .

We infer from Fig. 13, that critical strength in the thermodynamic limit is given by 0.1196 with an error of ± 0.009 , which is off from the expected value of zero. We attribute this error to the computation of the ground states due to the finite size of lattices used, thereby leading to a effective error in the entropy computation. Therefore, we conclude that in this case, the MES method fails to properly classify the topological phase transition.

VI. SUMMARY AND DISCUSSIONS

We have analyzed the robustness of topological order for the toric code in an open boundary setting under a perturbation by studying various properties. We see that the open boundary scenarios with perturbation can be classified into two classes, namely, the condensing and non-condensing classes depending on whether the excitations generated by the perturbation get confined or identified at the boundary. Both the condensing and non-condensing classes have been mapped to effective Ising models and thus, these models help provide critical insight into the nature of the phase transition. To further verify and consolidate the results from the effective Ising models, especially for the condensing case, we have studied the behavior of energy gap, TEE and the MES in the exact models. Using the above results we have made an attempt to numerically benchmark the MES method for detecting the phase transition.

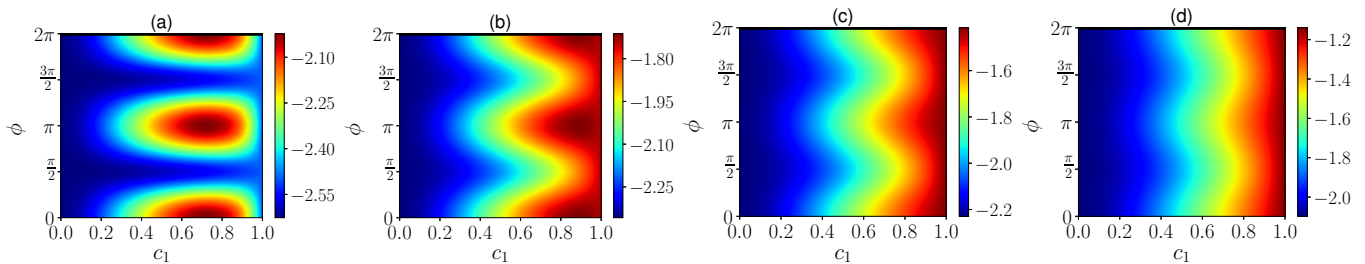


Figure 11. (a) Renyi-2 entropy of the state $|\eta\rangle = c_1 |\psi_1\rangle + c_2 e^{i\phi} |\psi_2\rangle$ depending on c_1 and ϕ at a perturbative strength of $h = 0.15$, As the perturbation is increased to $h = 0.25$ (b), $h = 0.29$ (c), and eventually $h = 0.33$ (d), one sees the two minima giving way to a single minimum at $\phi = 0, \pi$. ($N=20$ spins)

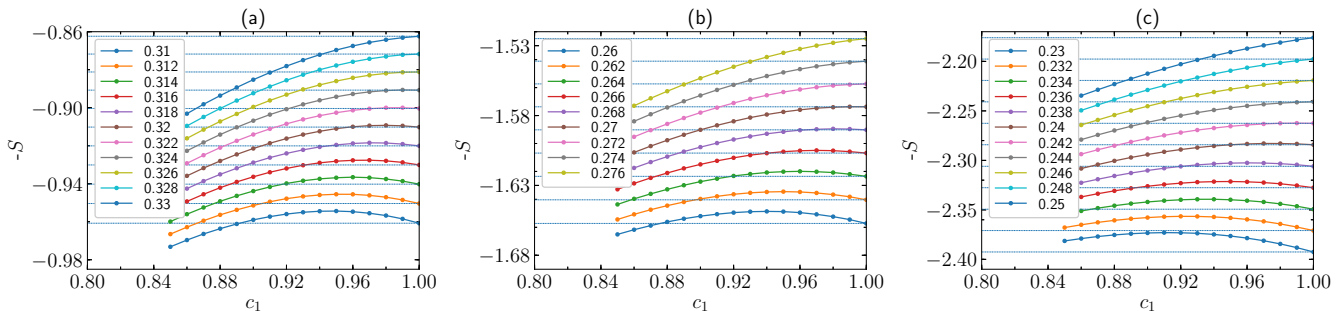


Figure 12. Renyi-2 entropy versus c_1 at different strengths, captured for different lattice sizes 15 (a), 20 (b), 25 (c). In the case where the entropy at $c_1=1$ forms a tangent to the entropy versus c_1 curve (computed at different strength) we denote the critical strength at which the second minimum disappears.

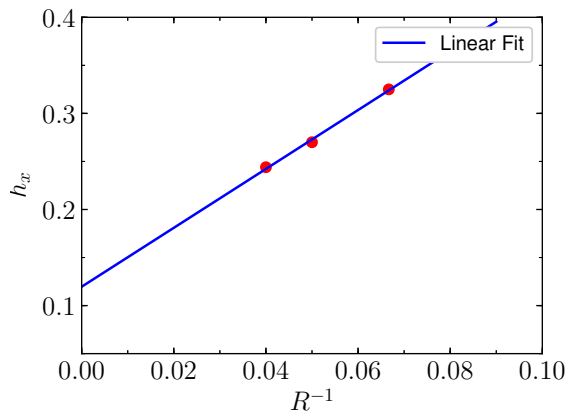


Figure 13. Finite size scaling of the critical strength where the second minimum in the Renyi-2 entropy disappears.

In an open boundary setting with a non-condensing scenario, we see that the critical strength occurs at $h = 0.453$ and we conclude that topological order in such systems is more robust when compared to the toric code in a periodic boundary setting under perturbation, which has a critical strength of $h = 0.328$ ³⁵. For the condensing class, the topological order breaks as soon as the pertur-

bation is turned on, i.e., for $h > 0$ there is no topological order.

In this paper, we have presented robustness under perturbation in an open boundary setting by choosing a cylinder with identical boundary conditions on either boundaries. It is also possible to construct a scenario, wherein we can identify the open boundaries of the cylinder with different boundary conditions, resulting in a mixed boundary. It would be interesting to explore the behavior of other signatures, for example expectation values of Wilson loop operators. It is also possible to interpolate from a toric code on torus to a toric code on cylinder with mixed boundaries by changing the underlying topology. We know that both the ground states are topologically ordered and it would be interesting to study different signatures which signal such a phase transition. One other interesting scenario would be to study the robustness of topological order in systems with domain wall under the effect of perturbation.

ACKNOWLEDGEMENTS

We thank Ling-Yan Hung for fruitful discussions. This work was funded by the Volkswagen Foundation, by the DFG within SFB 1227 (DQ-mat) and SPP 1929 (GiRyd),

by the Thousand Young Talents Program, and by the JSPS Grant-In Aid within a JSPS fellowship (P17023).

Appendix A: Mapping Toric code in open boundary setting under perturbation to associated Ising models

Group as boundary, $K = Z_2$, with $\sum_i \sigma_x^i$ as perturbation— The Hamiltonian is given by H_{grpx} . We note that in the case of group as boundary, the B_p violation condenses on the boundary. For perturbation, $H_p = \sum_i \sigma_x^i$, we note the following relations

$$\begin{aligned} [H_p, A_v] &= 0, \forall v \in \text{bulk}, \\ [H_p, A_{v'}] &= 0, \forall v' \in \text{boundary}, \\ [H_p, B_p] &\neq 0 \end{aligned}$$

The perturbation anticommutes with the B_p terms and therefore, we shift to the excitation space where the B_p violations are identified at the center of each face by a spin- $\frac{1}{2}$ allowing us to consider the effective Hamiltonian

$$H_{isgb} = -h_x \sum_{p,q} \mu_p^x \mu_q^x - h_x \sum_{p' \in \text{boundary}} \mu_{p'}^x - \sum_p \mu_p^z. \quad (\text{A1})$$

The motivation behind H_{isgb} is that the excitations generated by the perturbation appear in pairs in the bulk and are captured by nearest neighbor Ising interaction, while at the boundary the excitations can exist independently, which is captured by the additional term $h_x \sum_{p' \in \text{boundary}} \mu_{p'}^x$.

The following map captures the essence of the equivalence under the constraint that energy required to generate A_v violations is set to infinity.

$$\begin{aligned} H_{grpx} &= - \sum_p B_p - h_x \sum_i \sigma_x^i \\ H_{isgb} &= - \sum_p \mu_p^z - h_x \sum_{p,q} \mu_p^x \mu_q^x - h_x \sum_{p' \in \text{boundary}} \mu_{p'}^x \end{aligned}$$

Similar arguments can be constructed for the other Hamiltonian H_{idpz} which results in a condensing scenario. Instead of shifting to the excitation space of B_p , we shift to the excitation space of A_v where excitations are identified at vertices with a spin- $\frac{1}{2}$.

To summarize, we note that Hamiltonians H_{idpz} and H_{grpx} are equivalent in the Ising picture and correspond to the condensing class, whose Hamiltonian is given by

$$H_{ci} = -h_p \sum_{i,j} \mu_i^x \mu_j^x - h_p \sum_{k \in \text{boundary}} \mu_k^x - \sum_i \mu_i^z. \quad (\text{A2})$$

Group as boundary, $K = Z_2$, with $\sum_i \sigma_z^i$ as perturbation— The Hamiltonian is given by H_{grpz} . For perturbation $H_p = \sum_i \sigma_z^i$, we note the following relations

$$\begin{aligned} [H_p, B_p] &= 0, \forall p, \\ [H_p, A_v] &\neq 0, \forall v \in \text{bulk}, \\ [H_p, A_{v'}] &\neq 0, \forall v' \in \text{boundary}, \end{aligned}$$

We observe that A_v violations appear in pairs due to the perturbation and shifting to the excitation space where A_v violations are identified at the vertices by a spin- $\frac{1}{2}$, we have the following Ising Hamiltonian

$$H'_{isgb} = -h_z \sum_{v,w} \mu_v^x \mu_w^x - \sum_v \mu_v^z. \quad (\text{A3})$$

Again, the motivation for this effective Ising Hamiltonian is that the excitations generated by the perturbation appear in pairs in the bulk and are captured by nearest neighbor Ising interaction as above. Here, this nearest neighbor interaction is preserved at the boundary as the excitations are contained at the boundary. Therefore, this type of boundary does not support isolated excitations at the boundary. In the same way as above, we can capture the equivalence of the models by the following map

$$\begin{aligned} H_{grpz} &= - \sum_v A_v - h_z \sum_i \sigma_z^i \\ H'_{isgb} &= - \sum_v \mu_v^z - h_x \sum_{v,w} \mu_v^x \mu_w^x \end{aligned}$$

On similar lines, we can analyze the Hamiltonian H_{idpx} , where we move to the excitation space of B_p and identify each excitation with a spin- $\frac{1}{2}$ positioned at the center of the face.

To summarize, we note that Hamiltonians H_{idpx} and H_{grpz} are equivalent and form the non-condensing class whose Hamiltonian is given by :

$$H_{nci} = -h_p \sum_{i,j} \mu_i^x \mu_j^x - \sum_i \mu_i^z. \quad (\text{A4})$$

Appendix B: CNOT mechanism in the context of open boundaries

We present the CNOT mechanism which maps the Hamiltonian H_{grpx} to the equivalent Ising picture along with the topological spins and vacancy. This section heavily relies on the derivation mentioned in Ref. 36 and we extend the below map on top of the existing literature mentioned in the above reference.

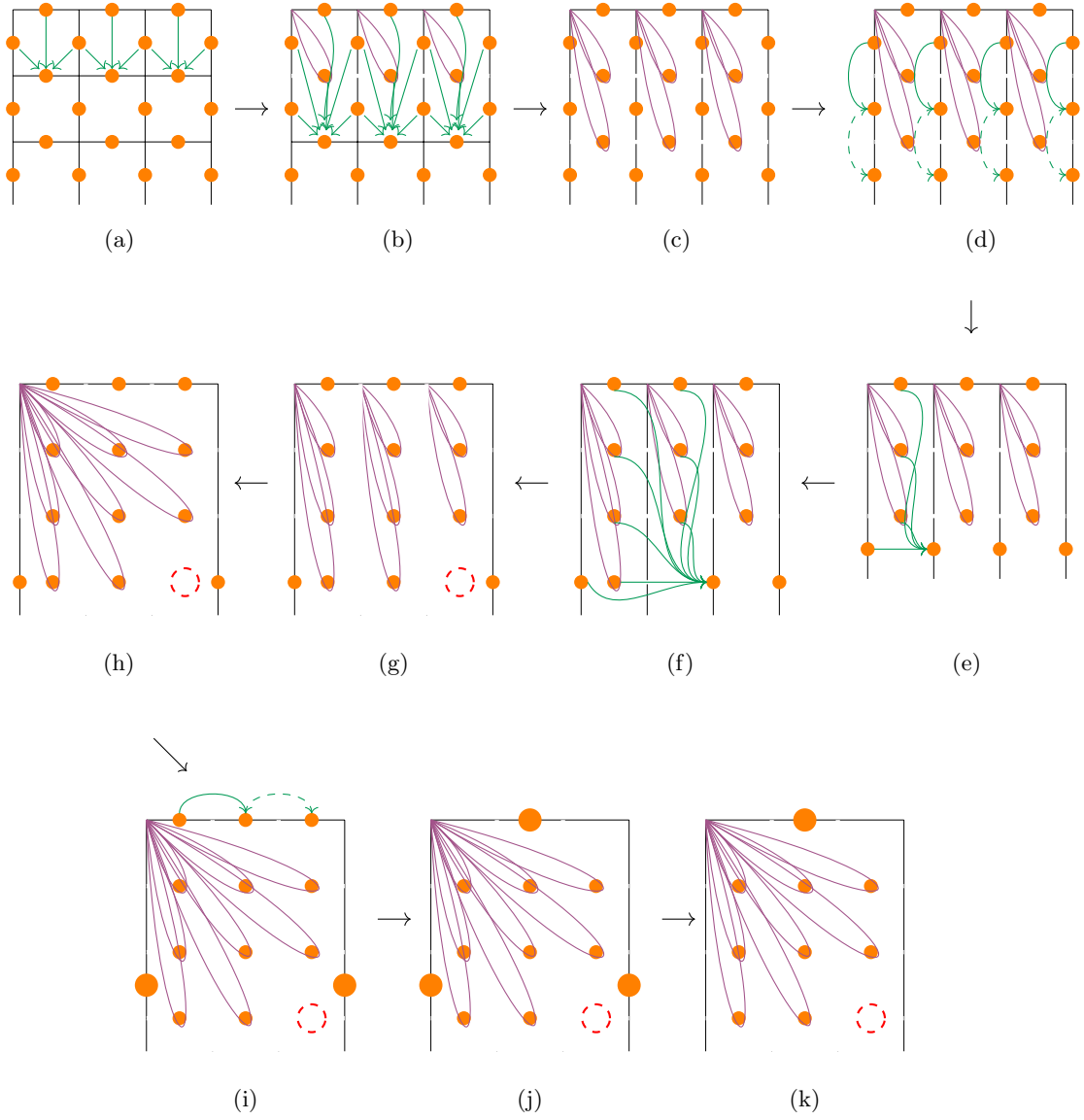


Figure 14. Ising map along with the topological spins (denoted by large orange dots) and the vacancy (denoted by dashed red circle) for Hamiltonian H_{grpx} . We note that all the above steps are as outlined in Ref. 36. The difference between the map in the periodic case and the open boundary case arises in (f), where the last rung is retained because of the boundary. Step (j) is equivalent to (k) since the action of two vertical non-trivial loop operators (homotopic loop operators) on the system have no effective action, $L_{topological}^2 = \mathbb{I}$, where $L_{topological}$ is the non-trivial loop operator in the vertical direction. Thereby the only loop operator remaining is in the horizontal direction connecting both the boundaries as indicated in (k). The topological spin in the horizontal direction couples the Ising spins on either side of the shorter boundary.

* amit.jamadagni@itp.uni-hannover.de

† bhattacharyya.arpan@yahoo.com

¹ M. H. Freedman, P/NP, and the quantum fieldcomputer, Proc. Natl. Acad. Sci. USA, **95**, 98 (1998).

² M. Freedman, A. Kitaev, M. Larsen, and Z. Wang, Topological quantum computation, Bull. Am. Math. Soc. **40**, 31 (2003).

³ C. Nayak, S. H. Simon, A. Stern, M. Freedman, and

S. Das Sarma, Non-Abelian anyons and topological quantum computation, Rev. Mod. Phys. **80**, 1083 (2008).

⁴ X. G. Wen, Vacuum degeneracy of chiral spin states in compactified space, Phys. Rev. B **40**, 7387 (1989).

⁵ X. G. Wen and Q. Niu, Ground-state degeneracy of the fractional quantum Hall states in the presence of a random potential and on high-genus Riemann surfaces, Phys. Rev. B **41**, 9377 (1990).

- ⁶ X. G. Wen, Topological orders in rigid states, *Int. J. Mod. Phys. B* **04**, 239 (1990).
- ⁷ L.-M. Duan, E. Demler, and M. D. Lukin, Controlling Spin Exchange Interactions of Ultracold Atoms in Optical Lattices, *Phys. Rev. Lett.* **91**, 090402 (2003).
- ⁸ A. Micheli, G. K. Brennen, and P. Zoller, A toolbox for lattice-spin models with polar molecules, *Nature Phys.* **2**, 341 (2006).
- ⁹ G. Jackeli and G. Khaliullin, Mott Insulators in the Strong Spin-Orbit Coupling Limit: From Heisenberg to a Quantum Compass and Kitaev Models, *Phys. Rev. Lett.* **102**, 017205 (2009).
- ¹⁰ C.-Y. Lu, W.-B. Gao, O. Gühne, X.-Q. Zhou, Z.-B. Chen, and J.-W. Pan, Demonstrating Anyonic Fractional Statistics with a Six-Qubit Quantum Simulator, *Phys. Rev. Lett.* **102**, 030502 (2009).
- ¹¹ H. Weimer, M. Müller, I. Lesanovsky, P. Zoller, and H. P. Büchler, A Rydberg quantum simulator, *Nature Phys.* **6**, 382 (2010).
- ¹² A. E. B. Nielsen and K. Mølmer, Topological matter with collective encoding and Rydberg blockade, *Phys. Rev. A* **82**, 052326 (2010).
- ¹³ H. Weimer, M. Müller, H. P. Büchler, and I. Lesanovsky, Digital quantum simulation with Rydberg atoms, *Quant. Inf. Proc.* **10**, 885 (2011).
- ¹⁴ J. T. Barreiro, M. Müller, P. Schindler, D. Nigg, T. Monz, M. Chwalla, M. Hennrich, C. F. Roos, P. Zoller, and R. Blatt, An open-system quantum simulator with trapped ions, *Nature* **470**, 486 (2011).
- ¹⁵ A. G. Fowler, M. Mariantoni, J. M. Martinis, and A. N. Cleland, Surface codes: Towards practical large-scale quantum computation, *Phys. Rev. A* **86**, 032324 (2012).
- ¹⁶ H. Weimer, Quantum simulation of many-body spin interactions with ultracold polar molecules, *Mol. Phys.* **111**, 1753 (2013).
- ¹⁷ D. Becker, T. Tanamoto, A. Hutter, F. L. Pedrocchi, and D. Loss, Dynamic generation of topologically protected self-correcting quantum memory, *Phys. Rev. A* **87**, 042340 (2013).
- ¹⁸ M. Sameti, A. Potočnik, D. E. Browne, A. Wallraff, and M. J. Hartmann, Superconducting quantum simulator for topological order and the toric code, *Phys. Rev. A* **95**, 042330 (2017).
- ¹⁹ S. Beigi, P. W. Shor, and D. Whalen, The Quantum Double Model with Boundary: Condensations and Symmetries, *Commun. Math. Phys.* **306**, 663 (2011).
- ²⁰ A. Kitaev and L. Kong, Models for Gapped Boundaries and Domain Walls, *Commun. Math. Phys.* **313**, 351 (2012).
- ²¹ L.-Y. Hung and Y. Wan, Generalized ADE classification of topological boundaries and anyon condensation, *J. High Energy Phys.* **2015**, 120 (2015).
- ²² I. Cong, M. Cheng, and Z. Wang, Topological Quantum Computation with Gapped Boundaries and Boundary Defects, [arXiv:1710.07197](https://arxiv.org/abs/1710.07197) (2017).
- ²³ I. Cong, M. Cheng, and Z. Wang, Universal Quantum Computation with Gapped Boundaries, *Phys. Rev. Lett.* **119**, 170504 (2017).
- ²⁴ B. Yoshida, Gapped boundaries, group cohomology and fault-tolerant logical gates, *Ann. Phys. (N. Y.)* **377**, 387 (2017).
- ²⁵ M. A. Levin and X.-G. Wen, String-net condensation: A physical mechanism for topological phases, *Phys. Rev. B* **71**, 045110 (2005).
- ²⁶ S. Trebst, P. Werner, M. Troyer, K. Shtengel, and C. Nayak, Breakdown of a Topological Phase: Quantum Phase Transition in a Loop Gas Model with Tension, *Phys. Rev. Lett.* **98**, 070602 (2007).
- ²⁷ A. Hamma and D. A. Lidar, Adiabatic Preparation of Topological Order, *Phys. Rev. Lett.* **100**, 030502 (2008).
- ²⁸ S. Dusuel, M. Kamfor, R. Orús, K. P. Schmidt, and J. Vidal, Robustness of a Perturbed Topological Phase, *Phys. Rev. Lett.* **106**, 107203 (2011).
- ²⁹ C. Castelnuovo and C. Chamon, Quantum topological phase transition at the microscopic level, *Phys. Rev. B* **77**, 054433 (2008).
- ³⁰ A. Y. Kitaev, Fault-tolerant quantum computation by anyons, *Ann. Phys. (N. Y.)* **303**, 2 (2003).
- ³¹ A. Kitaev and J. Preskill, Topological Entanglement Entropy, *Phys. Rev. Lett.* **96**, 110404 (2006).
- ³² M. Levin and X.-G. Wen, Detecting Topological Order in a Ground State Wave Function, *Phys. Rev. Lett.* **96**, 110405 (2006).
- ³³ S. Bravyi and A. Kitaev, Quantum codes on a lattice with boundary, [arXiv:quant-ph/9811052](https://arxiv.org/abs/quant-ph/9811052) (1998).
- ³⁴ J. Vidal, S. Dusuel, and K. P. Schmidt, Low-energy effective theory of the toric code model in a parallel magnetic field, *Phys. Rev. B* **79**, 033109 (2009).
- ³⁵ F. Wu, Y. Deng, and N. Prokof'ev, Phase diagram of the toric code model in a parallel magnetic field, *Phys. Rev. B* **85**, 195104 (2012).
- ³⁶ L. Tagliacozzo and G. Vidal, Entanglement renormalization and gauge symmetry, *Phys. Rev. B* **83**, 115127 (2011).
- ³⁷ M. Schuler, S. Whitsitt, L.-P. Henry, S. Sachdev, and A. M. Läuchli, Universal Signatures of Quantum Critical Points from Finite-Size Torus Spectra: A Window into the Operator Content of Higher-Dimensional Conformal Field Theories, *Phys. Rev. Lett.* **117**, 210401 (2016).
- ³⁸ J. L. Cardy, *Scaling and Renormalization in Statistical Physics* (Cambridge University Press, Cambridge, 1996).
- ³⁹ J. C. Wang and X.-G. Wen, Boundary degeneracy of topological order, *Phys. Rev. B* **91**, 125124 (2015).
- ⁴⁰ H.-C. Jiang, Z. Wang, and L. Balents, Identifying topological order by entanglement entropy, *Nature Phys.* **8**, 902 (2012).
- ⁴¹ C. Chen, L.-Y. Hung, Y. Li, and Y. Wan, Entanglement Entropy of Topological Orders with Boundaries, [arXiv:1804.05725](https://arxiv.org/abs/1804.05725) (2018).
- ⁴² Y. Chepeš, L. Cevolani, and S. Kehrein, Exact description of the boundary theory of the Kitaev Toric Code with open boundary conditions, [arXiv:1803.10217](https://arxiv.org/abs/1803.10217) (2018).
- ⁴³ Y. Zhang, T. Grover, A. Turner, M. Oshikawa, and A. Vishwanath, Quasiparticle statistics and braiding from ground-state entanglement, *Phys. Rev. B* **85**, 235151 (2012).
- ⁴⁴ W. Zhu, D. N. Sheng, and F. D. M. Haldane, Minimal entangled states and modular matrix for fractional quantum Hall effect in topological flat bands, *Phys. Rev. B* **88**, 035122 (2013).
- ⁴⁵ S. C. Morampudi, C. von Keyserlingk, and F. Pollmann, Numerical study of a transition between \mathbb{Z}_2 topologically ordered phases, *Phys. Rev. B* **90**, 035117 (2014).